Laser induced surface acoustic wave combined with phase sensitive optical coherence tomography for superficial tissue characterization

Li, Chunhui; Guan, Guangying; Zhang, Fan; Nabi, Ghulam; Wang, Ruikang K.; Huang, Zhihong

Published in:
Biomedical Optics Express

DOI:
10.1364/BOE.5.001403

Publication date:
2014

Document Version
Publisher's PDF, also known as Version of record

Biomedical Optics EXPRESS

Laser induced surface acoustic wave combined with phase sensitive optical coherence tomography for superficial tissue characterization: a solution for practical application

Chunhui Li,[1] Guangying Guan,[2,3] Fan Zhang,[2] Ghulam Nabi,[1] Ruikang K. Wang,[2,3] and Zhihong Huang[2,*]

[1]*Division of Imaging Technology, School of Medicine, University of Dundee, Dundee DD1 9SY, Scotland, UK*
[2]*School of Engineering, Physics and Mathematics, University of Dundee, Dundee DD1 4HN, Scotland, UK*
[3]*Department of Bioengineering, University of Washington, 3720 15th Ave NE, Seattle, WA 98195, USA*
z.y.huang@dundee.ac.uk

Abstract. Mechanical properties are important parameters that can be used to assess the physiologic conditions of biologic tissue. Measurements and mapping of tissue mechanical properties can aid in the diagnosis, characterisation and treatment of diseases. As a non-invasive, non-destructive and non-contact method, laser induced surface acoustic waves (SAWs) have potential to accurately characterise tissue elastic properties. However, challenge still exists when the laser is directly applied to the tissue because of potential heat generation due to laser energy deposition. This paper focuses on the thermal effect of the laser induced SAW on the tissue target and provides an alternate solution to facilitate its application in clinic environment. The solution proposed is to apply a thin agar membrane as surface shield to protect the tissue. Transient thermal analysis is developed and verified by experiments to study the effects of the high energy Nd:YAG laser pulse on the surface shield. The approach is then verified by measuring the mechanical property of skin in a Thiel mouse model. The results demonstrate a useful step toward the practical application of laser induced SAW method for measuring real elasticity of normal and diseased tissues in dermatology and other surface epithelia.

OCIS codes: (240.6690) Surface waves; (280.3375) Laser induced ultrasonics; (350.5030) Phase velocity; phase sensitive optical coherence tomography (PhS-OCT).

References and links

1. T. R. Tilleman, M. M. Tilleman, and M. H. Neumann, "The elastic properties of cancerous skin: Poisson's ratio and Young's modulus," Isr. Med. Assoc. J. **6**(12), 753–755 (2004).
2. Zhang, X. Kinnick, R. R. Pittelkow, and M. R. J. F. Greenleaf, 2008 Skin viscoelasticity with surface wave method, *2008 IEEE International Ultrasonics Symposium Proceedings*.
3. Nakajima M., Kiyohara Y., Shimizu M. and Kobayashi M. 2007 "Clinical application of real-time tissue elastography on skin lesions", MEDIX Suppl., 36–39.
4. J. D. Krehbiel, J. Lambros, J. A. Viator, and N. R. Sottos, 2008 "Digital Image Correlation for Improved Detection of Basal Cell Carcinoma", Proceedings of the XIth nternational Congress and Exposition.
5. Melanoma skin cancer," American Cancer Society, *http://www.cancer.org/acs/groups/cid/documents/webcontent/003120-pdf*, (2011)
6. Skin cancer," American Cancer Society, *http://www.cancer.org/acs/groups/content/@nho/documents/document/skincancerpdf.pdf*, (2007)
7. P. Ciarletta, L. Foret, and M. Ben Amar, "The radial growth phase of malignant melanoma: multi-phase modelling, numerical simulations and linear stability analysis," J. R. Soc. Interface **8**(56), 345–368 (2011).
8. A. F. Fercher, W. Drexler, C. K. Hitzenberger, and T. Lasser, "Optical coherence tomography – principles and

#205935 - $15.00 USD Received 5 Feb 2014; revised 24 Mar 2014; accepted 25 Mar 2014; published 3 Apr 2014

applications," Rep. Prog. Phys. **66**(2), 239–303 (2003).
9. P. H. Tomlins and R. K. Wang, "Theory, developments and applications of optical coherence tomography," J. Phys. D Appl. Phys. **38**(15), 2519–2535 (2005).
10. C. Sun, B. Standish, and V. X. Yang, "Optical coherence elastography: current status and future applications," J. Biomed. Opt. **16**(4), 043001 (2011), doi:10.1117/1.3560294.
11. J. M. Schmitt, "OCT elastography: imaging microscopic deformation and strain of tissue," Opt. Express **3**(6), 199–211 (1998).
12. R. C. Chan, A. H. Chau, W. C. Karl, S. Nadkarni, A. S. Khalil, N. Iftimia, M. Shishkov, G. J. Tearney, M. R. Kaazempur-Mofrad, and B. E. Bouma, "OCT-based arterial elastography: robust estimation exploiting tissue biomechanics," Opt. Express **12**(19), 4558–4572 (2004).
13. J. Rogowska, N. A. Patel, J. G. Fujimoto, and M. E. Brezinski, "Optical coherence tomographic elastography technique for measuring deformation and strain of atherosclerotic tissues," Heart **90**(5), 556–562 (2004).
14. H. J. Ko, W. Tan, R. Stack, and S. A. Boppart, "Optical coherence elastography of engineered and developing tissue," Tissue Eng. **12**(1), 63–73 (2006).
15. R. K. K. Wang, Z. H. Ma, and S. J. Kirkpatrick, "Tissue Doppler optical coherence elastography for real time strain rate and strain mapping of soft tissue," Appl. Phys. Lett. **89**(14), 144103 (2006).
16. S. J. Kirkpatrick, R. K. Wang, and D. D. Duncan, "OCT-based elastography for large and small deformations," Opt. Express **14**(24), 11585–11597 (2006).
17. X. Liang, A. L. Oldenburg, V. Crecea, E. J. Chaney, and S. A. Boppart, "Optical micro-scale mapping of dynamic biomechanical tissue properties," Opt. Express **16**(15), 11052–11065 (2008).
18. R. K. Wang, S. Kirkpatrick, and M. Hinds, "Phase-sensitive optical coherence elastography for mapping tissue microstrains in real time," Appl. Phys. Lett. **90**(16), 164105 (2007).
19. Kennedy, B.F.; Kennedy, K.M.; Sampson, D.D., "A review of optical coherence elastography: fundamentals, techniques and prospects," IEEE J. Sel. Top. Quantum Electron. **20**(2), 1–17 (2014).
20. R. K. Wang and A. L. Nuttall, "Phase-sensitive optical coherence tomography imaging of the tissue motion within the organ of Corti at a subnanometer scale: A preliminary study," J. Biomed. Opt. **15**(5), 056005 (2010).
21. S. Song, Z. Huang, T. M. Nguyen, E. Y. Wong, B. Arnal, M. O'Donnell, and R. K. Wang, "Imaging of tissue shear modulus by direct visualization of propagating acoustic waves with phase sensitive optical coherence tomography," J. Biomed. Opt. **18**(12), 121509 (2013).
22. S. Song, Z. Huang, and R. K. Wang, "Tracking mechanical wave propagation within tissue using phase-sensitive optical coherence tomography: Motion artifact and its compensation," J. Biomed. Opt. **18**(12), 121505 (2013).
23. T. M. Nguyen, S. Song, B. Arnal, E. Y. Wong, Z. Huang, R. K. Wang, and M. O'Donnell, "Shear wave pulse compression for dynamic elastography using phase-sensitive optical coherence tomography," J. Biomed. Opt. **19**(1), 016013 (2014).
24. B. F. Kennedy, T. R. Hillman, R. A. McLaughlin, B. C. Quirk, and D. D. Sampson, "In vivo dynamic optical coherence elastography using a ring actuator," Opt. Express **17**(24), 21762–21772 (2009).
25. B. F. Kennedy, X. Liang, S. G. Adie, D. K. Gerstmann, B. C. Quirk, S. A. Boppart, and D. D. Sampson, "In vivo three-dimensional optical coherence elastography," Opt. Express **19**(7), 6623–6634 (2011).
26. G. Guan, C. Li, Y. Ling, J. B. Vorstius, R. P. Keatch, R. K. Wang, and Z. H. Huang, "Quantitative evaluation of degenerated tendon model using combined optical coherence elastography and acoustic radiation force method," J. Biomed. Opt. **18**(11), 111417 (2013).
27. C. H. Li, Z. H. Huang, and R. K. K. Wang, "Elastic properties of soft tissue-mimicking phantoms assessed by combined use of laser ultrasonics and low coherence interferometry," Opt. Express **19**(11), 10153–10163 (2011).
28. C. Li, G. Guan, Z. Huang, M. Johnstone, and R. K. Wang, "Noncontact all-optical measurement of corneal elasticity," Opt. Lett. **37**(10), 1625–1627 (2012).
29. C. Li, G. Guan, R. Reif, Z. Huang, and R. K. Wang, "Determining elastic properties of skin by measuring surface waves from an impulse mechanical stimulus using phase-sensitive optical coherence tomography," J. R. Soc. Interface **9**(70), 831–841 (2012).
30. C. Li, G. Guan, X. Cheng, Z. Huang, and R. K. Wang, "Quantitative elastography provided by surface acoustic waves measured by phase-sensitive optical coherence tomography," Opt. Lett. **37**(4), 722–724 (2012).
31. C. Li, G. Guan, S. Li, Z. Huang, and R. K. Wang, "Evaluating elastic properties of heterogeneous soft tissue by surface acoustic waves detected by phase-sensitive optical coherence tomography," J. Biomed. Opt. **17**(5), 057002 (2012).
32. C. B. Scruby and L. E. Drain, *Laser Ultrasonics: Techniques and Applications* (Hilger Press, Bristol 1990).
33. D. H. Hurley and J. B. Spicer, "Line source representation for laser-generated ultrasound in an elastic transversely isotropic half-space," J. Acoust. Soc. Am. **116**(5), 2914–2922 (2004).
34. P. A. Doyle and C. M. Scala, "Near-field ultrasonic Rayleigh waves from a laser line source," Ultrasonics **34**(1), 1–8 (1996).
35. S. Kenderian, B. B. Djordjevic, and R. E. Green, Jr., "Point and Line Source Laser Generation of Ultrasound for Inspection of Internal and Surface Flaws in Rail and Structural Materials," Res. Nondestruct. Eval. **13**(4), 189–200 (2001).
36. American National Standard Institute, Safety of laser products – Part 1: Equipment classification, requirements and user's guide, IEC 60825–1, Edition 1.2 (2001–08).
37. W. Sun, Y. Peng, and J. Xu, "A de-noising method for laser ultrasonic signal based on EMD," J. Sandong Univ. **38**, 1–6 (2008).

#205935 - $15.00 USD Received 5 Feb 2014; revised 24 Mar 2014; accepted 25 Mar 2014; published 3 Apr 2014

38. H. C. Wang, S. Fleming, Y. C. Lee, S. Law, M. Swain, and J. Xue, "Laser ultrasonic surface wave dispersion technique for non-destructive evaluation of human dental enamel," Opt. Express **17**(15), 592– 607 (2009).
39. K. D. Mohan and A. L. Oldenburg, "Elastography of soft materials and tissues by holographic imaging of surface acoustic waves," Opt. Express **20**(17), 18887–18897 (2012).
40. D. Schneider, B. Schultrich, H. J. Scheibe, H. Ziegele, and M. Griepentrog, "A laser-acoustic method for testing and classifying hard surface layers," Thin Solid Films **332**(1-2), 157–163 (1998).

1. Introduction

The majority of pathological changes in the surface of organs such as skin results in the change of elastic properties and/or thickness of the affected layers. For examples, different types of skin cancer such as squamous cell carcinomas and malignant melanomas would have increased stiffness while basal cell carcinomas tends to have decreased Young's modulus of affected skin tissue [1–3]. Generally, stage I skin cancer affects the epidermis and upper dermis layer, while stage II skin cancer involves the whole dermis layer and possibly the upper subcutaneous fat layer. These conditions would lead to the increase of epidermis and dermis layer thicknesses [4–7]. Early diagnosis and treatment can improve the survival rate up to 90%-100% for stage I and ~50%~85% for stage II [1, 3, 5, 6]. Currently, the treatment and diagnosis of many dermatological conditions are largely carried out on a visual basis by trained dermatologists. Similarly in case of gastrointestinal and urothelial cancers in urology, depth of cancer remains important information necessary for clinical decision making. To accurately carry this out the clinician requires years of extensive training and experience. There are however a number of conditions that are not easily diagnosed or monitored by human eye alone when it requires detecting small changes in the thickness and mechanical properties of the skin layers. Thus, a non-intrusive, non-invasive elastography method that can accurately measure mechanical properties *in vivo* is required.

A number of techniques have been developed for the evaluation of the mechanical properties of skin. Optical coherence elastography (OCE) takes advantages of high resolution of optical coherence tomography (OCT) [8, 9], has been widely studied to evaluate the skin mechanical properties both qualitatively and quantitatively [10–19]. Currently, the majority of OCE techniques use speckle tracking [11–14] and phase-sensitive approaches [15–18] to monitor the tissue mechanical responses from stretching, compressing, or excited vibration by an external actuator [20–23]. Kennedy *et al.* used a specially designed sample arm that combined with a ring actuator to excite vibration within tissue sample, and then used OCT to detect signals from the same side of the samples [24]. The approach can successfully differentiate and calculate the different strain responses in skin epidermis and dermis layers. More recently, the 3D elastography of human skin was reported using this method [25] with high axial and lateral resolution. Quantitative measurement of this method can also be achieved by the assumption of uniform stress distribution [26]. However, the depth that this elastography method can achieve is limited by the OCT imaging depth of the tissue, which is less than 1.5mm (can only reach to upper layer of dermis). These attributes limits its clinical application to the measurement of superficial skin diseases. Our group was the first to combine impulse stimulated surface acoustic waves (SAWs) method with the phase sensitive OCT (PhS-OCT) to quantitatively evaluate the elastic properties of layered agar phantoms, *ex vivo* primate cornea and *in vivo* human skin [27–31]. Here, the PhS-OCT is used to remotely measure the SAW signals propagating on the sample surface. The generated broad-band SAWs have the nature of dispersion, i.e. different frequency contents penetrate into different depth with different velocities, thus, quantitative elastic information of different layers of a sample can be obtained by analyzing dispersion curve of SAW phase velocity. Different from the method of Kennedy *et al.*, the sensing depth of our method only relies on the bandwidth of a SAW signal measured by PhS-OCT system. The system is shown to be suitable for characterization of elastic properties of thick layered tissues (~4-5mm) [30].

Among different kinds of SAWs stimulations, high energy Q-switched laser pulse can be used as a remote, non-contact and non-destructive excitation source to generate SAWs

#205935 - $15.00 USD Received 5 Feb 2014; revised 24 Mar 2014; accepted 25 Mar 2014; published 3 Apr 2014

propagating on soft tissues [27, 28]. However, it is still a problem to directly apply this method on to tissue because of the complex mechanisms and potential safety issues when applying high energy laser pulse, e.g. tissue thermal damage. Meanwhile, in many cases, a high energy stimulating laser pulse is necessary to generate a detectable SAW in the far field relative to the location of laser stimulation. This study proposes a novel, yet practical solution for laser induced SAWs used in tissue elasticity measurement. A thin layer of black agar membrane is applied to the tissue of interest for: 1) acting as a surface shield to protect tissue from heat generation due to the irradiation of laser pulse; 2) increasing the absorption of laser pulse in order to generate SAWs with better signal-to-noise ratio (SNR). In this study, the depth-resolved temperature distribution of black agar phantom induced by the laser pulse is detected and recorded by a thermal camera. The maximum increased temperature and heat impacted depth are analyzed under different laser pulse energy. Then the thickness of black agar membrane is determined to ensure that the laser induced temperature increase in sample would not affect the integrity of soft tissue sample. We show that this method is feasible to provide the bulk quantitative Young's modulus value of *in vivo* human skin and tissues, promising clinical use in the diagnosis, treatment and management of different kinds of pathological conditions.

2. Theoretical background

When a material is illuminated with a short laser pulse, the optical power that is absorbed by the material is converted to heat, which leads to rapid localized rise in temperature. The absorbed optical energy is depended on the laser wavelength and the optical properties of the material. The optical intensity variation with depth inside an absorbing medium that is illuminated by a light beam at normal incidence is given by an exponential decay relation [32]:

$$I(x,y,z,t) = I_0(x,y,t)\exp\ [-\gamma z] \tag{1}$$

where $I_0(x,y,t)$ is the incident intensity distribution at the surface which is a function of the laser parameters. γ is the absorption coefficient of the material under the wavelength of light pulse. The optical penetration depth is defined as 1/γ. Compared to metallic material, the absorption coefficient of soft material is much smaller. Thus the optical penetration depth can be much larger. The optical energy absorbed by the material leads to a distributed heat source in the material given by:

$$q(x,y,z,t) = \gamma I(x,y,z,t) = \gamma I_0(x,y,t)\exp(-\gamma z) \tag{2}$$

The absorbed optical energy has similar spatial and temporal characteristics to the incident laser source. Assuming the absorbed optical energy is 100% converted into the thermal energy, the conversion leads to temperature rise within local tissue volume at the depth of z. For numerical convenience, it can be solved using the equation of heat conduction equation to solve the thermal source distribution:

$$\frac{k}{C_{th}^{\ 2}}\frac{\partial^2 T}{\partial t^2} + \rho C\frac{\partial T}{\partial t} = k\nabla^2 T + q \tag{3}$$

where T is the temperature, ρ is the density, C is heat capacity, k is the thermal diffusivity, and C_{th} is the thermal wave speed usually taken as equal to the longitudinal wave speed of the material.

The localized increase in temperature results in rapid thermal expansion and generation of different mechanical waves. Among these waves, SAWs propagate along the material surface with amplitudes that decay exponentially with depth. Each wave component propagates with

#205935 - $15.00 USD Received 5 Feb 2014; revised 24 Mar 2014; accepted 25 Mar 2014; published 3 Apr 2014

its own velocity, and the impulse is deformed as it propagates along the material. It is the concentration of the wave energy at the material surface that makes the SAWs very sensitive to layered materials like skin. In layered material the velocity of SAW depends on frequency, which is known as dispersion. For a homogeneous and isotropic material described by Young's Modulus E, Poisson's Ratio v, and density ρ, the phase velocity can be described by [27]:

$$C_R = \frac{0.87 + 1.12v}{1+v}\sqrt{\frac{E}{2\rho(1+v)}} \tag{4}$$

In a multi-layered material where the elastic properties of the layers are different, the effect of all these layers affects the propagation velocity of the SAWs, with the phase velocity dispersion curves dependent on the elastic parameters, density and layer thickness. Longer wavelength (lower frequency) SAWs have deep penetration depth and propagate with a velocity dependent on the deeper layers, while the shorter wavelength (higher frequency) SAWs have low penetration depth and propagate with a velocity dependent on the surface layers. The penetration depth is approximately one wavelength of its associated SAWs, which is inversely related to the frequency of the wave [30, 31]:

$$z \approx \lambda = \frac{C_R}{f} \tag{5}$$

where z indicates the penetration depth, λ is the SAW wavelength of the corresponding frequency of f.

3. Materials and methods

3.1 Surface shield and mouse skin tissue

In this study, we used 1% agar phantom for agar membrane, acting as the surface shield to protect the material beneath from thermal heating. 5% India ink was added to it during the manufacturing procedures. It aimed to make the phantom black for increasing the absorption coefficient to the high energy laser pulse. Higher laser energy being absorbed indicates higher amplitude of SAW being generated. In order to analyze the full depth, a 1% agar phantom was produced with thickness of 5mm which is thick enough for obtaining the full depth-resolved thermal distribution of agar. Before the thermal experiment, the phantom was sealed and placed in the laboratory for 12 hours to reach the environment temperature of 298.8K.

By determining the depth of thermal effect from laser pulse, the thickness of agar membrane can be determined and produced. It will then be placed on Thiel mice cadavers for skin elasticity measurement. Mice cadavers embalmed by Thiel's method were processed in the Centre for Anatomy and Human Identification at the University of Dundee, United Kingdom. Thiel mice cadavers are embalmed in a water-based solution of salts for fixation, boric acid for disinfection, glycol, chlorocresol and ethanol, and a very small amount of formaldehyde. The skin is life-like flexibility, joints are fully flexible. Six mice cadavers embalmed by Thiel's method were used. The experiment carried on the same skin area of mid medial back of the mice cadaver. The measurement repeated for 5 times for each of the mice cadaver with and without agar membrane for cross-validation.

3.2 Generation and detection of SAWs

The system set up for generation and detection of laser-induced SAW in surface shield protected skin tissue is shown in Fig. 1.

#205935 - $15.00 USD Received 5 Feb 2014; revised 24 Mar 2014; accepted 25 Mar 2014; published 3 Apr 2014

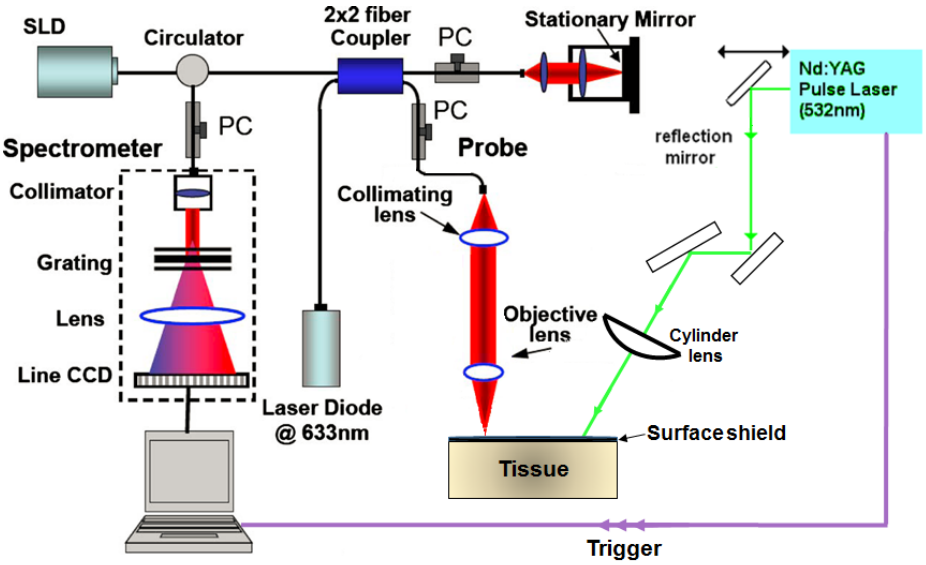

Fig. 1. Schematic of system setup consisting of laser SAW generation and PhS-OCT detection parts with a surface shield on tissue sample.

A solid state Nd:YAG laser (~532 nm central wavelength) (Continuum Surelite Laser) was used as the high energy laser pulse source for SAW generation. The short laser pulse was with duration of 6 ns and repetition rate of 0.2 Hz (5s). During the experiment, the laser irradiation on the sample was at an angle of 35°. Before subjecting sample to laser pulses, a cylindrical lens was employed to generate a line source with approximately constant energy distribution in the length direction. The line extent was ~2-2.5mm and Gaussian distribution in the width direction with a radius of ~150μm. Compared with the focused laser pulse, the line source significantly reduced irradiated power density on the sample. Thus, more energy can be injected into the specimen, permitting an improved signal/noise ratio for the measurement of SAW-forms compared with that of a circularly symmetric source [33–35]. In order to record the dispersion of laser-induced SAW, several detecting locations with a known separation distances are required by this technology. Here, we mounted the reflection mirror and cylindrical lens on a translation stage, so that the excitation laser beam was translated to the required distances for the measurement of generated SAW signals.

A Jade infrared thermal camera ThermoIMAGER TIM 160 (MICRO-EPSILON) was used to record the temperature field caused by the high energy laser pulse. The camera has 160 × 120 pixels (pixels size of 0.19mm) with the highest integration time of ~8μs and noise level of 0.1K. The camera collected data in free run mode, because the trigger mode has inherent 1s's delay which is longer for transient thermal analysis. The data from thermal camera was transferred to the PC for further processing. The energy detector, FieldMaster Laser Power & Energy Meter (COHERENT) was used to record the energy of the laser pulse at the tissue surface before each experiment. Half of the line source irradiated onto the sample surface (as shown in Fig. 2), thus highest laser energy irradiated to the sample was half of the laser output energy. Thermal camera was set to record the side of sample, thus the depth-resolved thermal effect to laser pulse can be collected and analyzed.

#205935 - $15.00 USD Received 5 Feb 2014; revised 24 Mar 2014; accepted 25 Mar 2014; published 3 Apr 2014

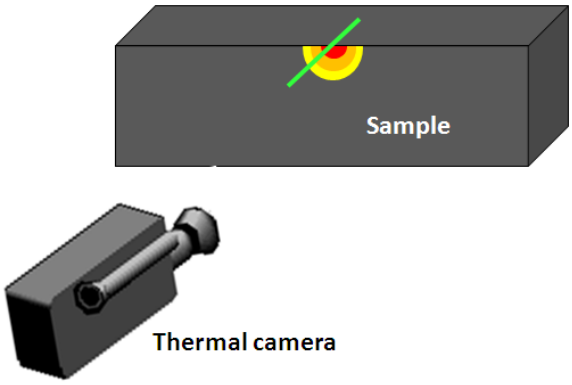

Fig. 2. Diagram of experimental thermal analysis

Soft tissue laser irradiation safety parameters are defined by American National Standards Institute (ANSI) standard IEC 60825-1 [36]. To avoid permanent tissue damage, the maximum permissible exposure (MPE) which is defined as the level of laser radiation to the tissue exposed without hazardous effects of biological changes in the tissue. The MPE values are specified in units of Jm^{-2} (radiant exposure) and depend on the laser wavelength, exposure energy, duration, and tissue type. For skin tissue under the condition proposed in this study the MPE value is 200 Jm^{-2}. Thus, above the maximum MPE value, laser induced SAW method is not safe to apply directly on human skin. In this case, a surface membrane is then needed to shield laser induced temperature rise. In this study, a series of laser energy was set from 2 mJ to 34 mJ for (corresponding to 13 Jm^{-2} to 452 Jm^{-2}) for thermal analysis. For each laser energy, five thermal data sets were collected and analyzed. Thermal affected depth above the maximum MPE value (200 Jm^{-2}) is important parameter to determine the thickness of surface membrane.

The detection of SAW signals was accomplished by a PhS-OCT system. It has been described in details previously [26–29]. The system allows detection of SAW signals for tissue elastic properties measurement and imaging of sample microstructures and membrane thickness simultaneously. The thickness of protective membrane and different layers of tissue is important in this study since it provides as a cross validation for phase velocity curve analysis of SAW method. Briefly, the PhS-OCT system employed a superluminecent diode as the light source, with a center wavelength of ~1310 nm and a bandwidth of ~46 nm, implemented by a spectral domain configuration. The sample arm used an objective lens of ~50 mm focal length to deliver the probing light on the tissue surface coupled with the wave signals into the PhS-OCT. The acquisition rate was determined by the spectrometer employed in the system that had a maximum rate of ~47,000 A-scans per second. For SAW signal detection, the system was triggered to record the signal when Nd:YAG laser pulse was emitted. M-mode acquisition was used and at the each location, 1024 A-scans were acquired to obtain one M-mode scan.

4. Data processing

For the elasticity analysis, SAWs were detected and recorded on sample surface at six locations with the same step length (0.5mm/step) between adjacent locations. For each detection point, ten measurements were made and averaged to reduce the random noise. The signal's noise was minimized by using a Hilbert–Huang method that reduces the low and high frequency noise [37].

The phase velocity dispersion curve between any two measured signals, $y_1(t)$ and $y_2(t)$ corresponding to locations x_1 and x_2, respectively, were analyzed. The phase difference $\Delta\varphi$ between the SAW signals $y_1(t)$ and $y_2(t)$ was calculated by determining the phase of the cross-

#205935 - $15.00 USD Received 5 Feb 2014; revised 24 Mar 2014; accepted 25 Mar 2014; published 3 Apr 2014

power spectrum $Y_{12}(f)$. The phase difference can be computed directly from the two complex spectra:

$$y_1 \xrightarrow{F} Y_1(f) = A_1(f)e^{i\varphi_1(f)} \tag{6}$$

$$y_2 \xrightarrow{F} Y_2(f) = A_2(f)e^{i\varphi_2(f)} \tag{7}$$

and it gives the phase of the cross-power spectrum, $Y_{12}(f)$:

$$Y_{12}(f) = Y_1(f) \cdot \overline{Y_2(f)} = A_1 A_2 e^{i(\varphi_2 - \varphi_1)} \tag{8}$$

$$\Delta\varphi = \varphi_2 - \varphi_1 \tag{9}$$

where $Y_1(f)$ and $Y_2(f)$ are the Fourier transformations of $y_1(t)$ and $y_2(t)$, A_1 and A_2 are the amplitude of cross-power spectrum and $\Delta\varphi = \varphi_1 - \varphi_2$ is the phase difference between the measured signals $y_1(t)$ and $y_2(t)$. Given two receivers at a known distance ΔX, the measured phase difference is 2π when the propagating wave has a wavelength that equals the distance ΔX. More in general, the ratio between the phase difference and 2π equals the ratio between the distance and the wavelength:

$$\Delta\varphi / 2\pi = \Delta X / \lambda \tag{10}$$

If the distance between the receivers and the phase difference between the two corresponding signals has been measured, the wavelength can be computed as:

$$\lambda = \Delta X \cdot 2\pi / \Delta\varphi \tag{11}$$

The phase velocity is then obtained, given the frequency f, as:

$$C_R = \lambda \cdot f \tag{12}$$

Thus, the phase velocity can be expressed as:

$$C_R = \Delta X \cdot 2\pi \cdot f / \Delta\varphi \tag{13}$$

The phase velocity is then computed from the phase difference between the signals at two receivers. Both the autocorrelation spectrum and the phase velocity dispersion curves are the key parameters for our analyses, as the former provides the available frequency range of the signals, while the latter provides the elastic and structural information of the samples. The cut-off frequency for the surface waves has been defined at −20 dB from the maximum of the autocorrelation spectrum, where the uncertainty of the dispersion curves are increased [38].The final phase-velocity dispersion curve was determined by averaging all the phase velocities between two detection points.

#205935 - $15.00 USD Received 5 Feb 2014; revised 24 Mar 2014; accepted 25 Mar 2014; published 3 Apr 2014

5. Results and discussions

4.1 Thermal analysis between 1% black agar phantom and high energy laser pulse

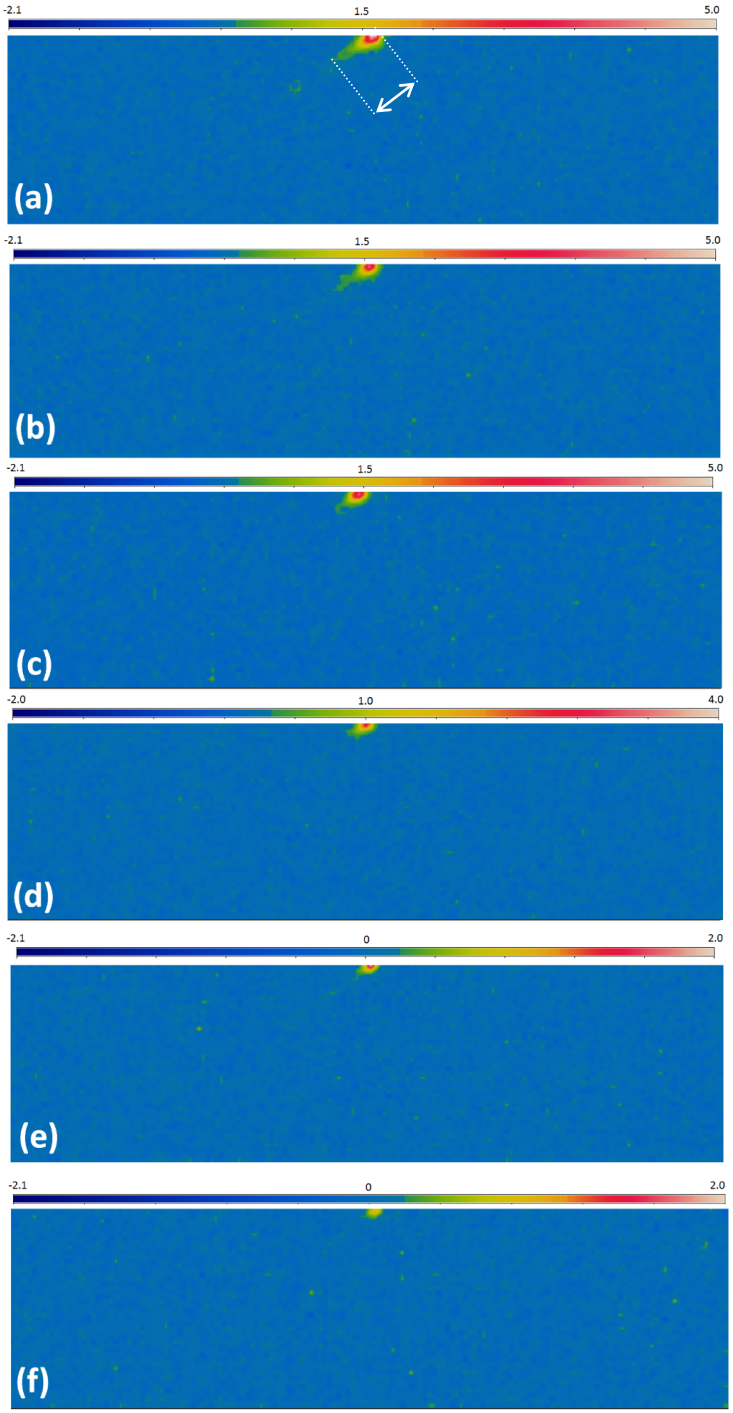

Fig. 3. Typical depth-resolved thermal distribution of 1% black agar phantom under the laser pulse energy of (a) 34mJ, (b) 28mJ, (c) 20mJ, (d) 14mJ, (e) 5mJ and (f) 2mJ with maximum increased temperature, the unit of color bar is K.

#205935 - $15.00 USD Received 5 Feb 2014; revised 24 Mar 2014; accepted 25 Mar 2014; published 3 Apr 2014

Figure 3(a)-3(f) shows typical depth-resolved thermal distribution induced by different energy of laser pulses (a-34mJ, b-28mJ, c-20mJ, d-14mJ, e-5mJ and f-2mJ) in the time with maximum raised temperature. Figures show the difference in values instead of absolute value for better demonstration of increase in temperature. Clearly from Fig. 3, higher laser energy induces higher temperature, and thermal effects diffused deeper and into lager area. Different from material with high absorption coefficient, e.g. metal, laser energy is absorbed over a much larger volume and diffuses deep into surrounding area in soft tissue phantoms instead of a thin surface layer. Because there is an angle of 35° between laser beam and phantom surface, the thermal diffusion area also has an angle. Thus in this case, we choose the direction of laser irradiation for the maximum thermal impact depth analysis (marked in Fig. 3(a)). The impacted depth is the distance between laser pulses irradiating point to the raised thermal value of 0.1K, which reaches to the noise level of thermal camera. The value of impacted depths under different laser energy is summarized in Table 1.

The highest temperature occurred in the center of the laser beam on the material surface. Increased temperature curves under different laser energy in the center of laser beam are shown in Fig. 4(a). Compared to metallic material, laser induced heating and cooling process in soft phantom is relatively slow. It normally takes ~24 μs for induced temperature reaches its highest value and ~2 ms for the temperature to drop to environment temperature. Figure 4(b) shows approximate linear relationship between laser pulse energy and maximum raised temperature. It also has been summarized in Table 1.

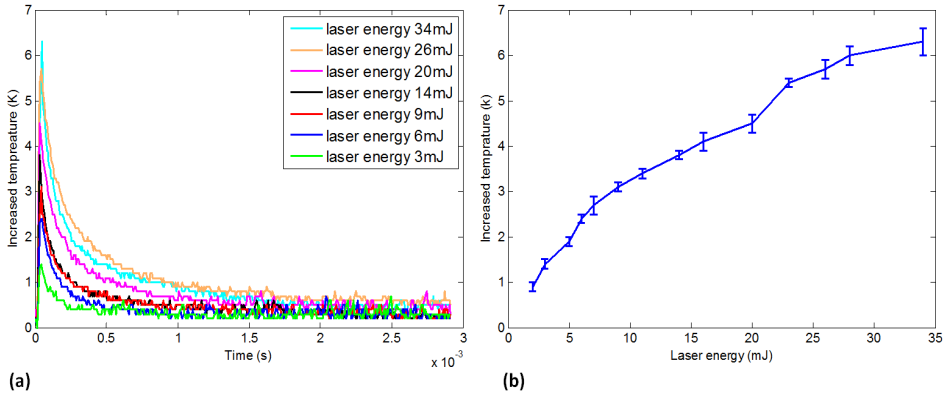

Fig. 4. (a) Laser pulse induced heating and cooling procedures in 1% agar phantom under different laser energy; (b) the relationship between laser energy and maximum raised temperature.

#205935 - $15.00 USD Received 5 Feb 2014; revised 24 Mar 2014; accepted 25 Mar 2014; published 3 Apr 2014

Table 1. Thermal and mechanical effect of agar phantom to different energy of laser pulse

Laser energy (mJ)	Radiant exposure (J/m^2)	Maximum thermal impacted depth (mm)	Maximum increased temperature (K)	Detectable SAW from 2mm to laser source (Y/N)
34	452	3.04	6.3 ± 0.3	
28	372	2.47	6.0 ± 0.2	
26	345	2.09	5.7 ± 0.2	
23	306	1.9	5.4 ± 0.1	
20	266	1.71	4.5 ± 0.2	
16*	213*	1.33	4.1 ± 0.2	
14	186	1.33	3.8 ± 0.1	
11	146	1.14	3.4 ± 0.1	
9	120	1.14	3.1 ± 0.1	
7	93	0.95	2.7 ± 0.2	
6	80	0.95	2.4 ± 0.1	
5	67	0.95	1.9 ± 0.1	
3	40	0.76	1.4 ± 0.1	
2	27	0.57	0.9 ± 0.1	Y

After analyzing maximum temperature induced by laser and depth as summarized, we choose a laser pulse with energy of ~16mJ for Thiel mouse cadaver skin elasticity measurement (marked in Table 1) in the experiments that follows. In this case the radiant exposure value is higher than maximum acceptable value defined by American National Standards Institute (ANSI) standard IEC 60825-1. In this energy level, the maximum induced heat is ~4.1K and the impacted depth is ~1.33mm. In order to successfully shield the thermal effect caused by the laser pulse, a ~1.5mm's black agar membrane which has the same ingredients with agar phantom in the thermal experiment is produced. The size of the membrane is $10x10mm^2$ which is large enough to detect SAW from different locations. To avoid thermal expansion area, SAWs are detected from 2mm to the laser pulse. SAWs can be detected under a very low laser energy, i.e. under 2mJ which cause a temperature raising of ~0.9K. No SAW could be detected under the temperature rising below 0.1K in this study.

#205935 - $15.00 USD Received 5 Feb 2014; revised 24 Mar 2014; accepted 25 Mar 2014; published 3 Apr 2014

4.2 Skin elasticity analysis using Thiel mouse cadavers applied with agar membrane

The imaging mode of the PhS-OCT system was first used to acquire cross-sectional microstructures images (B-scan) of the sample, immediately before the SAW experiments. Figure 5 shows the typical OCT image scanned from one male Thiel mouse cadaver covered by 1% black agar membrane with the thickness of ~1.5mm. Clearly the agar membrane can be differentiated from mouse tissues. The mouse cadaver has a thin layer of dermis and underlying subcutaneous fat layer. The structure imaging indicates there is no air bubble and gap in between mouse skin and agar membrane which otherwise would impact SAW's propagation.

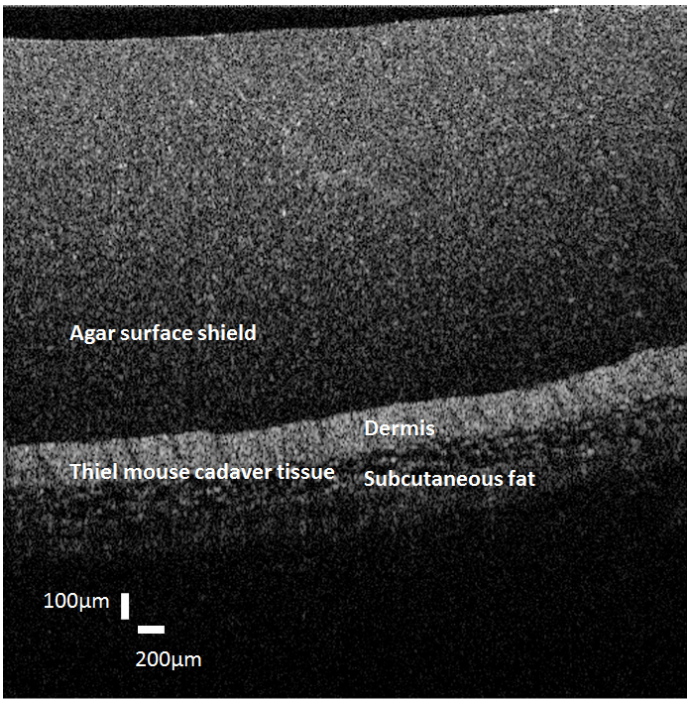

Fig. 5. Typical OCT image of Thiel mouse cadaver applied with 1% black agar membrane.

Figures 6 shows the typical SAW data measured from the mouse cadaver covered by agar membrane. The detection step was set to 0.5 mm, started from the location at 2mm away from the excitation and finished at the location 4.5 mm away from the excitation. Each signal waveform is purposely shifted vertically by equal distance in order to better illustrate the results captured at different positions. The horizontal dotted lines indicate the baseline. It can be seen that the SAW disperses as it travels and can be determined by a clear wave distortion when travelling away from source, indicating that the SAW was travelling in a heterogeneous medium, i.e. layered material.

#205935 - $15.00 USD Received 5 Feb 2014; revised 24 Mar 2014; accepted 25 Mar 2014; published 3 Apr 2014

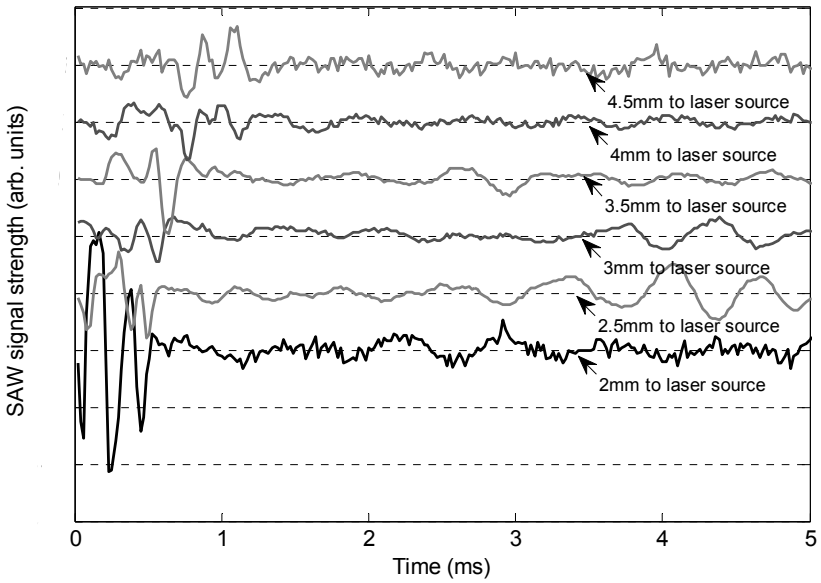

Fig. 6. SAW signal measured when it travels along mouse cadaver covered with agar membrane. The signal was measured initially at 2 mm position away from the excitation (bottom curve), and then sequentially stepped with 0.5 mm step size until 4.5 mm away from the excitation (top curve).

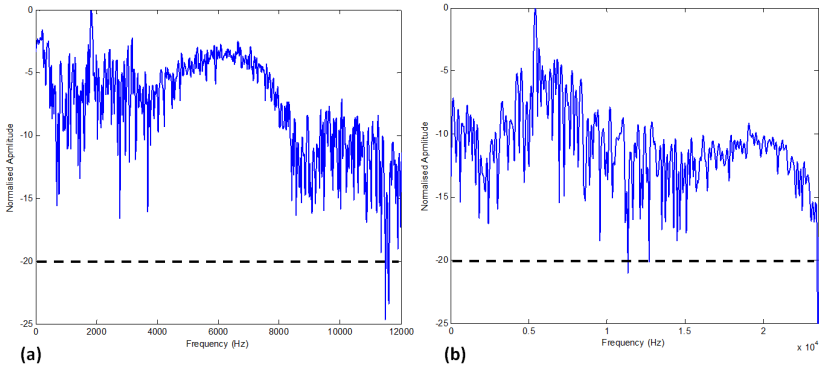

Fig. 7. Frequency spectrum of SAWs tested from of the same Thiel cadaver mouse with (a) and without (b) agar membrane

Both the autocorrelation spectrum and the phase-velocity dispersion curves of the detected SAWs are key parameters for our analyses, as the former provides the available frequency range of the signals, while the latter provides the elastic and structural information of the samples. In order to analyze the phase velocity curve correctly, the frequency range of SAW has to be determined first. Figure 7 shows the frequency spectrum of SAW tested from the same Thiel cadaver mouse with (a) and without (b) agar membrane. As mentioned previously, the cut-off frequency for the surface waves has been defined as −20 dB from the maximum of the autocorrelation spectrum. Based on this rule, the frequency range of SAW tested from mouse skin covered by membrane ranges from 0 to 12 kHz and that of SAW tested mouse skin without membrane ranges from 0 to 23.5 kHz.

The phase velocity dispersion curves of the Thiel mouse cadaver skin with and without agar membrane are presented and compared in Fig. 8(a) and Fig. 8(b). The phase velocity dispersion curves are not constant for all frequencies, since we were detecting a

#205935 - $15.00 USD Received 5 Feb 2014; revised 24 Mar 2014; accepted 25 Mar 2014; published 3 Apr 2014

heterogeneous material. In Fig. 8(a), the phase velocity of mouse cadaver skin with agar membrane increases and drops. This is expected since each layer of the mouse cadaver skin sample covered with agar membrane has different phase velocities. The initial phase velocity in low frequency (0-~1000Hz) represents the subcutaneous fat layer, with a value of ~2.92 m/s. The phase velocity increases at higher frequencies which represents the dermis layer of the mouse skin, finally reaching a plateau of ~7.58 m/s. These values indicate that the mouse dermis's Young's modulus is higher than subcutaneous fat. As the frequency increases, the phase velocity drops again due to the influence of the agar membrane. The phase velocity drop to ~4.51 m/s as the top layer of agar membrane has a 1% concentration. These results corroborate the theoretical expectations and our previous study [29–31], where the phase velocity at lower frequencies indicates the mechanical properties of deeper tissue layers, while the phase velocity at higher frequencies indicates the mechanical properties of the superficial layers. The results from Fig. 8(b) acts as a cross validation, in order to see the influence of membrane to the elasticity measurement. In Fig. 8(b), the sample is the same mouse cadaver skin without the agar membrane. As expected, the initial value of phase velocity curve is ~2.71m/s, and this value represents the subcutaneous fat of mouse skin. With the increase of frequency, the phase velocity increase to ~7.91m/s, represents to dermis layer of mouse skin.

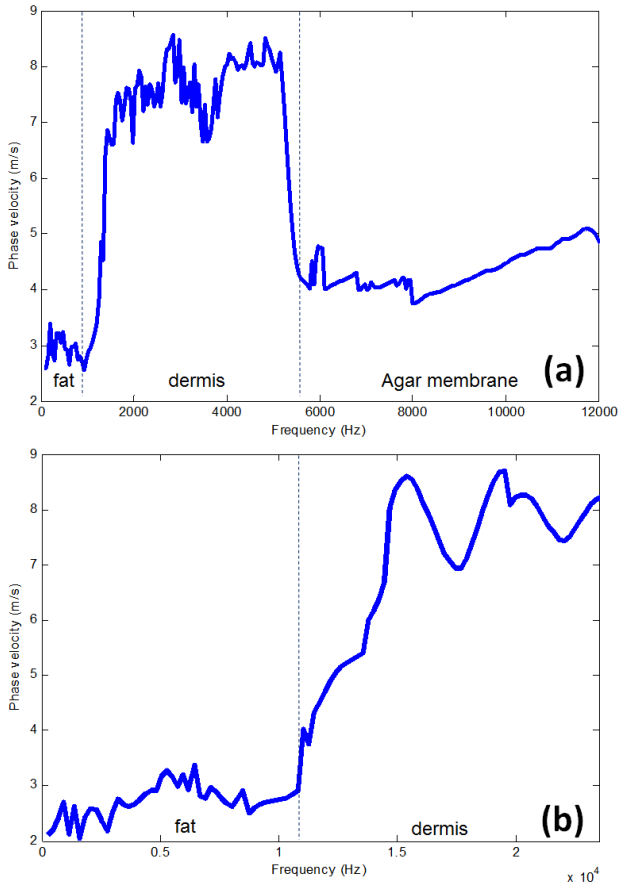

Fig. 8. Phase velocity dispersion curves of the same Thiel cadaver mouse with (a) and without (b) agar membrane.

Comparing Fig. 8(a) with 8(b), both of the phase velocity values of subcutaneous fat and dermis are approximately the same as expected. However, there is a significant frequency

#205935 - $15.00 USD Received 5 Feb 2014; revised 24 Mar 2014; accepted 25 Mar 2014; published 3 Apr 2014

shift between the two curves, e.g. the phase velocity of subcutaneous fat stops at ~1000Hz in Fig. 8(a) and ~10.7kHz in Fig. 8(b). It is likely due to the application of agar membrane that alters the relative depth of the sample. It is clear from Eq. (5) that the sample thickness and the frequency content within SAW exhibit a complicated relationship. The application of agar membrane on top of the skin tissue, thus, leads to change in the frequency content of phase velocity curves. However, the membrane does not cause significant change of phase velocity values of different skin layers. Note that the dermis phase velocity of mouse cadaver with membrane (Fig. 8(a)) is relatively lower than that without membrane (Fig. 8(b)). This is because the phase velocity of low frequency SAWs is not only dependent on the Young's modulus of deep layers, but is considered as a combination of all depths probed by the SAW [39]. Thus, the introduction of low stiffness membrane may affect the phase velocity of all the layers within sample. To simply the complication, we here assume that the phase velocity curve is depth-sectioning without the influence between each other in data analysis. We are currently developing a systematic inversion technique for the SAW method to mitigate this problem.

From the experiments above, the measured phase velocities for the Thiel mouse cadaver skin of all the six subjects are plotted in Fig. 9 with the average and standard deviations of the calculated Young modulus. To calculate the Young modulus, we averaged the phase velocity of the plateau which represents subcutaneous fat and dermis layers. Based on previous studies, we can assume that the Poisson ratio of the human skin tissue is approximately 0.48. We used approximately 1110 kg•m^{-3} as the dermis density and approximately 971 kg•m^{-3} as the subcutaneous fat density [40]. Therefore, with these measured phase-velocity values, we can calculate the Young modulus according to Eq. (4).

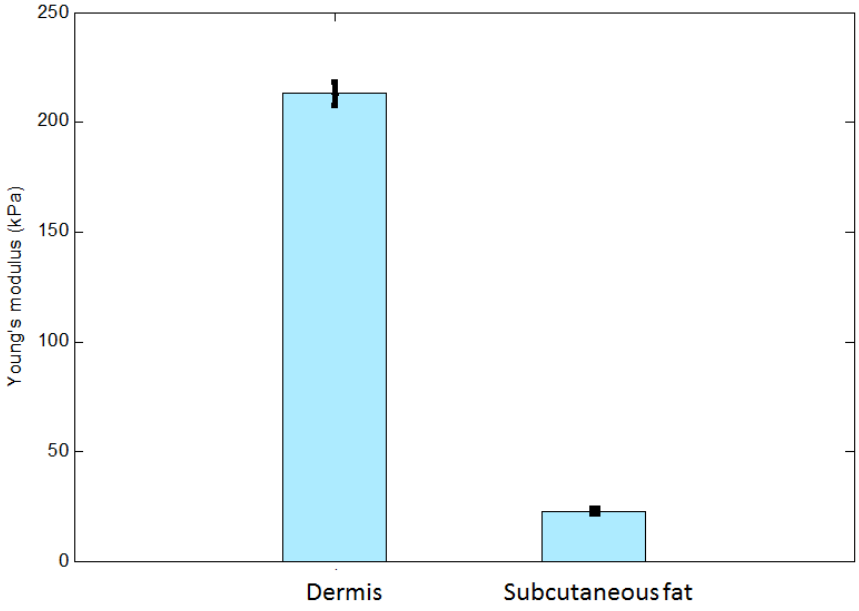

Fig. 9. Average Young's modulus from six Thiel mouse cadaver skin dermis and subcutaneous fat. The error bars denote standard deviation.

6. Discussions and conclusions

In this paper we have presented a novel solution using laser induced SAW to analyze the elasticity of soft tissues. A purpose-built black agar membrane can be applied on tissues in order to shield the heat generated by the high energy laser pulse. It can be concluded that the maximum temperature increment happens at the center of the laser spot which is dependent

#205935 - $15.00 USD Received 5 Feb 2014; revised 24 Mar 2014; accepted 25 Mar 2014; published 3 Apr 2014

on the laser pulse and is proportional with the laser energy. The depth of generated heat is important in this study because it determines the thickness of protective membrane. It can be obtained from depth-resolved thermal distribution recorded from a thermal camera. Combining protective membrane, high energy laser pulse and the PhS-OCT detector, the mechanical properties of Thiel mouse cadaver skin can be evaluated in a non-contact, non-invasive and non-destructive nature by calculating and analyzing the phase-velocity curves from the detected SAW signals. Experimental results from cadaver mouse skin with and without membrane are in good agreement. It indicates the application of agar membrane may not have significant impact on the elasticity measurement. However, contents of strong frequency shift occur because the membrane may change the relative depth of tissue layers.

This study demonstrates the feasibility of using surface membrane for laser induced SAW for evaluating elastic properties of layered soft solid materials and soft biological tissues, e.g. skin. The surface dyed membrane works to shield the heat when MPE exceed its maximum safe value, and improve the SNR of SAW.

Agar perhaps may not necessarily be the ideal material for the future application of this technique. However, different material of membrane has different optical and thermal properties, thus would exhibit different thermal effect to the laser pulse. This paper sets baseline and for any material the exact same experimental procedure should be done to determine the ideal depth of membrane. Ideally, the elasticity of membrane should be lower or equal to the elasticity of material it covers. A membrane with significantly higher elasticity than that tested here will prevent SAW from penetrating into the deep layer of sample.

The paper demonstrates that the technique could be translated into clinical settings, because the system is sensitive to the elastic and geometry changes of a sample. Since most skin diseases result in the changes of the elastic properties and/or thickness of the affected skin layer, this would cause changes in the phase-velocity curve, which can be detected by our system. The current system may have potential in diagnosing diseases of the dermis layer, such as level II skin cancer (including malignant melanoma, squamous cell carcinoma and basal cell carcinoma) and scleroderma. In addition, with a special designed contact lens, this method is also applicable in cornea elasticity measurement, thereby facilitating the determination of the intraocular pressure (IOP) when combined with appropriate biomechanical modelling. Similarly, technique could be used for endoscopic assessment of cancers in urinary bladder and gastrointestinal tract.

Acknowledgment

The authors would like to thank Mrs. Joyce Joy for providing the Thiel mouse cadavers.

#205935 - $15.00 USD Received 5 Feb 2014; revised 24 Mar 2014; accepted 25 Mar 2014; published 3 Apr 2014